INTERNATIONAL JOURNAL FOR NUMERICAL METHODS IN FLUIDS, VOL. 20, 1179–1197 (1995)

THE DEVELOPMENT OF A STRUCTURED MESH GRID ADAPTION TECHNIQUE FOR RESOLVING SHOCK DISCONTINUITIES IN UPWIND NAVIER–STOKES CODES

M. K. PATEL, K. A. PERICLEOUS AND S. BALDWIN*

Centre for Numerical Modelling and Process Analysis, University of Greenwich, London SE18 6PF, U.K.

Dedication. We humbly dedicate this work to the memory of our good friend and colleague Stephen Baldwin, who sadly died recently in an air-crash whilst performing his duties. Steve was the inspiration behind this project and his enthusiasm and dedication were noted by all who knew him. Given time, he would have reached far. He will be sadly missed.

SUMMARY

A technique is described for the adaptation of a structured control volume mesh during the iterative solution process of the Navier–Stokes equations. The scalar equidistribution method is adopted, in conjunction with a Laplace-like grid solver to make a curvilinear body-fitted grid sensitive to local flow gradients. Hence, whilst the total number of grid nodes remains constant during a computation, their relative position is continuously adjusted to promote clustering of cells in regions where gradients are high. The focus of this work is in compressible aerodynamics, where such clustering would be desirable in regions containing shocks but also in boundary layers. The technique is three-dimensional and operates in a series of user-defined grid subdomains or patches. These patches act as reference frames within which grid activity takes place. Bi-cubic splines are extensively used to define the aerodynamic surfaces forming the calculation boundaries and to ensure that grid movement does not compromise surface integrity. The technique is applied to aerofoils, wing surfaces, transonic ducts and nozzles and a supersonic wedge cascade. Significant sharpening of both normal and oblique shock discontinuities is demonstrated over static grid simulations and with fewer overall grid nodes. The technique is successful in both inviscid and viscous (turbulent) simulations.

KEY WORDS adaptive grids; equidistribution; compressible viscous aerodynamics; CFD modelling

INTRODUCTION

An adaptive grid capability is desirable in structured Navier–Stokes CFD codes which are used to compute the flow around aircraft flying at speeds close to that of sound. In this "transonic' regime, although the aircraft may be flying subsonically, pockets of supersonic flow exist over parts of the airframe. These pockets usually terminate in a shock wave, which causes a drag increase through pressure modification but also by causing local boundary layer thickening and separation.

* Formerly of British Aerospace (MAD), Farnborough, Hampshire GU16 6YU, U.K.

CCC 0271–2091/95/101179–19

Received October 1993
Revised July 1994

The transonic regime is notoriously difficult to model mathematically, not only because of shocks, in effect a discontinuity in the flow field, but also because regions of the flow alternate between elliptic and hyperbolic behaviour. Since the equations characterizing the three-dimensional flow around aircraft can only be solved numerically, the discrete formulation adopted has to be able to satisfy all the above requirements. Specialized techniques have been developed in this area of compressible aerodynamics which can be broadly divided into two main categories: those which mainly deal with areas in the flow which are not significantly influenced by viscosity or turbulent mixing, mainly in external aerodynamics, and those where viscosity and turbulent mixing or recirculation are important, such as engine intakes, wakes, overexpanded rocket nozzles and supersonic impinging jets (for V/STOL aircraft). In the first category the inviscid Euler equations are solved. Good shock-capturing capability is achieved through the use of explicit time marching, with artificial viscosity used to suppress oscillations (see References 1 and 2). In the second category the full Navier–Stokes equations need to be solved, where a pressure-correction-type technique[3] is usually adopted, modified for compressibility in various ways (see e.g. References 4–7). The present contribution is also concerned with Navier–Stokes solutions; however, a conventional upwind differencing scheme is employed as incorporated in the commercially available CFD code PHOENICS.[8] Dynamic grid adaptivity is used instead to 'sharpen-up' flow gradients and hence resolve flow discontinuities such as shocks where these occur.

The partial differential equations characterizing the problem are discretized on a solution grid which is generally curvilinear with mesh lines made to follow the contours of the aerodynamic surface. Furthermore, the grid is structured so that grid lines originating at a boundary will terminate at a boundary (for unstructured adaptive grid methods see References 9 and 10). A control volume convention is adopted[11] whereby flow variables are assumed constant within any cell and are physically placed in the cell centroid. Velocity components are staggered with respect to pressure to prevent spurious pressure oscillations in the solution.

Under these conditions the computational grid is gradually optimized as the field solution proceeds. An optimum grid is obtained when fine cells locate themselves in areas of high field gradients (e.g. shock waves, boundary layers) and moderate/large cells in areas of weaker gradients. Adaptive grids have long been in operation in unstructured grid FE-type codes where local grid refinement can be readily effected with the minimum of interaction with the main code structure. These codes have been used successfully in inviscid Euler calculations. For calculations where the effects of viscosity and turbulent flow cannot be neglected, Navier–Stokes solutions are necessary. The most widespread N–S codes in use in the aircraft industry are of the structured grid control volume type such as PHOENICS. These codes are often not specifically designed for transonic flow and unfortunately suffer from numerical smearing of shock discontinuities. The technique presented here offers a solution to this deficiency through dynamic grid refinement.

The authors have developed a technique for the automatic adaption of structured body-fitted grids in three dimensions, based loosely on the method of gradient equidistribution, whereby the product of the chosen field scalar gradient (e.g. pressure) and grid cell dimension in the direction of the gradient remains constant. Grid rearrangement by this method is followed by normalization to ensure that the overall domain dimensions are retained. Since cell vertices are not restricted but allowed to move quite independently of each other, highly skewed grids can result under certain conditions; to avoid this, the grid is then processed in a patch-wise manner through an iterative Laplace-like solver that promotes orthogonality. Boundary points are restricted to move along aerodynamic surfaces on predefined bicubic splines to ensure that surface integrity is not compromised. The technique was developed and tested as a modular attachment to the commercial CFD code PHOENICS, although it is not code-specific. The module can also operate independently, requiring as input the original curvilinear grid and the scalar field upon which adaption is to be based.

with normal or oblique shocks, in several flow situations such as a supersonic wedge cascade, a missile, a converging–diverging nozzle, an aerofoil, etc.

PRINCIPLES OF GRID ADAPTION

The basic concepts underlying grid adaptation in CFD are quite clear. Starting from a suitably chosen grid, a solution of the flow field is obtained and then this solution is used to compute a new grid on which the flow field is recalculated. The process is repeated many times in a given simulation until convergence is reached. The criteria governing grid movement need to be carefully examined to ensure that the additional overheads entailed in grid and geometry recalculation are justified in increased solution accuracy or perhaps increased flow field spatial resolution. The principle of cell equidistribution is adopted in this implementation, where the new cell dimensions are made inversely proportional to local field gradients (see e.g. References 12 and 13).

It should be recognized that the techniques used in unstructured finite element (FE) codes for this purpose[9,10] are quite unsuitable for use in structured (or even block-structured) control volume (CV) CFD codes. Grid freedom is restricted by the structuredness, since cells have their neighbours predefined at the onset and grid lines have to be continuous throughout the computational domain, starting at one boundary and terminating at the opposite one. Structured CV Navier–Stokes codes are used almost exclusively in the U.K. aircraft industry for flow situations where viscosity is important or alternatively where large portions of the flow field are turbulent (e.g. the flow around a V/STOL aircraft in hover[14]). It is for this reason that we are concerned with structured CV codes.

Having said the above, it should be emphasized that although the basic concepts of grid adaptation are quite simple, the actual implementation of a reliable, automatic, three-dimensional technique within the framework of a general-purpose CFD code remains a formidable undertaking. The following guiding principles have been identified as prerequisites for successful implementation:

1. The grid density in each co-ordinate direction becomes a function of the gradient of a selected flow variable (pressure, density, etc.) in that direction.
2. The grid is adjusted within the normal iterative sweep of the calculation at each time step, e.g. during a SIMPLE (or its variants)[15] type of pressure correction adjustment.
3. The user retains a measure of control on how, when, where and by how much the grid changes with each adjustment.
4. Grid lines must not collapse on to each other or cross over, or in other ways generate unsuitable cells.
5. Surface definition and integrity are not compromised at the boundaries; hence grid density is not only a function of flow gradient but also of geometric surface gradient.
6. Other 'good practices' of grid generation, i.e. orthogonality and reasonable cell aspect ratios, are not adversely affected by grid movement.
7. The ease of use of the main CFD package is not impaired by the addition of this facility.

During a simulation the total number of cells in each co-ordinate direction will remain constant. This is an additional restriction imposed on the method by the structure of PHOENICS, which does not allow access to the variable indexing routines during iteration. The user is, however, free to re-dimension his programme and restart if necessary after adding extra cells in his grid.

METHOD OF IMPLEMENTATION

The technique presented here is based on cell *equidistribution*, where new cell dimensions are taken to be inversely proportional to the flow field gradients. Hence in the x-direction this would give

$$\Delta x\left|\frac{\partial\phi}{\partial x}\right| = k \quad \text{or} \quad \Delta x = \frac{k}{|\partial\phi/\partial x|}, \tag{1}$$

where k is a constant, Δx is the new cell dimension and $\partial\phi/\partial x$ is the gradient of ϕ. This simple equation has several obvious shortcomings which make it impractical to use. It leads to infinity as the gradient tends to zero, there is no correlation between the new grid and the old one, and the user has no control over the extent of movement of the original nodes. To overcome the first two shortcomings, equation (1) can be modified as

$$\Delta x_n = \frac{k_x}{|\partial\phi/\partial x|_s + k_x}\,\Delta x_o, \tag{2}$$

where Δx_o is the original cell dimension, k_x is comparable in magnitude to $\partial\phi/\partial x$ and may be a function of $\partial\phi/\partial x$, and the subscript 's' denotes that the gradient is taken from a splined approximation of the discrete field gradient. Equation (2) possesses a number of desirable characteristics which make it suitable for use:

1. As $\partial\phi/\partial x \to 0$, $\Delta x_n \to \Delta x_o$ as required.
2. As $\partial\phi/\partial x \to \infty$, $\Delta x_n \to \varepsilon$, where ε is a small fraction of Δx_o.
3. The sensitivity of the grid movement to $\partial\phi/\partial x$ can be adjusted by choosing the relative magnitude of k and $\partial\phi/\partial x$. Hence, if $k \approx |\partial\phi/\partial x|_{\min}$, maximum movement occurs up to the limits imposed by grid fineness, whilst if $k \approx |\partial\phi/\partial x|_{\min}$, the maximum allowable grid movement would be max $\Delta x_n = 0{\cdot}5\Delta x_o$.

In practice the actual function used will depend on the type of problem tackled. Three possible functions have been considered:

$$k_x = \frac{1}{nx}\sum\left|\frac{\partial\phi}{\partial x}\right|, \tag{3a}$$

$$k_x = \frac{1}{nx(ny+1)(nz+1)}\sum\left|\frac{\partial\phi}{\partial x}\right|, \tag{3b}$$

$$k_x = \frac{1}{(ny+1)(nz+1)}\sum\left|\frac{\partial\phi}{\partial x}\right|_{\max}. \tag{3c}$$

In the first of these k is taken to be the average gradient along each line; in general its value will then differ between lines. In the second one, k is taken to be the average gradient over the entire field and in the last one, k is taken to be the average of the line gradient maxima averaged over all lines. The value of k determined by equations (3b) and (3c) applies over the whole grid, with nx, ny and nz being the numbers of cells in the x-, y- and z-directions respectively.

The characteristics of these alternative derivations of k can be inferred from the definitions given. Equation (3a) can lead to skewed grids especially when applied to cases with oblique shocks (e.g. the wedge cascade). Equation (3b), which takes the field average of the gradients, leads to a value of k that is small compared with the gradient peak. It is therefore too sensitive for flows with shocks and can lead to grid collapse if used without relaxation. Equation (3c), on the other hand, gives the best grid control in flows with shocks, but it is rather slow since it only allows a maximum cell contraction of one-half the previous grid dimension in any iteration.

Thus equation (2) also provides some control over the amount of grid movement along grid lines by judicious selection of the function k_x. To encourage the rapid transfer of cells from low-gradient to high-gradient areas of the flow field and at the same time to reduce the likelihood of cells collapsing, a new quantity is introduced in equation (2), the *cell contraction parameter* α_x which can take values between 0 and 1. The final equidistribution law then becomes

$$\Delta x_n = \left(\frac{k_x}{|\partial\phi/\partial x|_s + k_x} (1 - \alpha_x) + \alpha_x \right) \Delta x_o. \tag{4}$$

Examination of equation (4) shows that α_x is simply a linear relaxation parameter which only allows a partial correction of the original grid dimension for $0 < \alpha_x < 1$. Setting $\alpha_x = 0$ allows full cell contraction, whilst setting $\alpha = 1$ prevents any alteration of the original cell. Hence, if we define Δx_{max} and Δx_{min} to be the maximum and minimum allowable cell dimensions respectively, α_x can be defined in terms of these quantities as

$$\alpha_x = \frac{\Delta x_{max} - \Delta x_o}{\Delta x_{max} - \Delta x_{min}}, \tag{5}$$

so that as $\Delta x_o \to \Delta x_{min}$, $\alpha_x \to 1$ and the grid becomes 'stiff', resisting any further change; if, on the other hand, $\Delta x_o \to \Delta x_{max}$, $\alpha_x \to 0$ and full movement is permitted.

Equation (5) can be applied successively in the x-, y- and z-directions along each grid line to adapt the grid in three dimensions. Its behaviour is not dissimilar to that of an earthworm which proceeds along in a series of contractions and extensions of its segments; the final length of the grid line adapted will be shorter than the original and each line therefore needs to be expanded or *normalized* by multiplying every cell in it by the overall contraction ratio before proceeding to the next line.

Although the equidistribution equation (5) has been chosen by the authors as the most efficient for this implementation, other control functions are possible, e.g. those given in Figure 1 (W1–W9), some of which are reproduced from Reference 13. Notable among these are higher-order spatial gradients of the field variable q and the term in the square root, which are intended to account for grid curvature.

In the adaptive process, boundary vertices are treated in the same way as internal ones, with the difference that points move not in the co-ordinate direction but along the boundary surface. Certain boundary points on the surface are treated as 'fixed'; their position in the co-ordinate space must not be altered by grid movement; however, their grid index is allowed to vary. Such points act as markers which usually define positions of physical discontinuity along the boundary. The grid is allowed to progress through the markers, with the grid point closest to a marker being *captured* at the end of the move. Fixed points are also conveniently used to divide the mesh into subdomains (or patches); see e.g. Figure 2. These subdomains can then be used to perform a special action on part of the grid, such as orthogonalization, by solving a Laplace link equation for the internal vertex co-ordinates. Similar precautions need to be taken where solid obstacles are present within the computational domain. The grid is allowed to move through the obstacle as the flow surrounding it dictates, without altering its geometrical definition.

In summary, the adaptive process proceeds in the following manner.

(i) Adapt the grid in the main flow direction.
(ii) Normalize co-ordinate lines to the original length.
(iii) Slide boundary points along the bounding surface, following splines.
(iv) Re-index boundary points as they slide across geometric patches.
(v) Repeat (i)–(iv) in the other two directions (optional) or continue.
(vi) Orthogonalize the grid by solving a Laplace equation for the transverse grid co-ordinates in a patch-wise manner (optional).

* Equi-distribution:

$$W1 = 1 + \left|\frac{dq}{dS}\right| + \left|\frac{d^2q}{dS^2}\right| \qquad W2 = 1 + \left|\frac{dq}{dS}\right|$$

$$W3 = \left|\frac{dq}{dS}\right| \qquad W4 = \left|\frac{d^2q}{dS^2}\right|$$

$$W5 = 1 + \left|\frac{dq}{dS}\right| + 0.01\left|\frac{d^2q}{dS^2}\right| \qquad W6 = 1 + \left|\frac{d^2q}{dS^2}\right|$$

$$W7 = \sqrt{\left|\frac{d^2q}{dS^2}\right|} \qquad W8 = 1 + \left|\frac{dq}{dS}\right| + 0.01\frac{\left|\frac{d^2q}{dS^2}\right|}{\sqrt{(1 + (\frac{dq}{dS})^2)}}$$

$$W9 = 1 + \left|\frac{dq}{dS}\right| + \frac{\left|\frac{d^2q}{dS^2}\right|}{\sqrt{(1 + (\frac{dq}{dS})^2)}}$$

* A combination approach:

alpha(LAPLACE) + beta(POISSON) + gamma(EQUI) = 0

Figure 1. A collection of equidistribution weighting functions

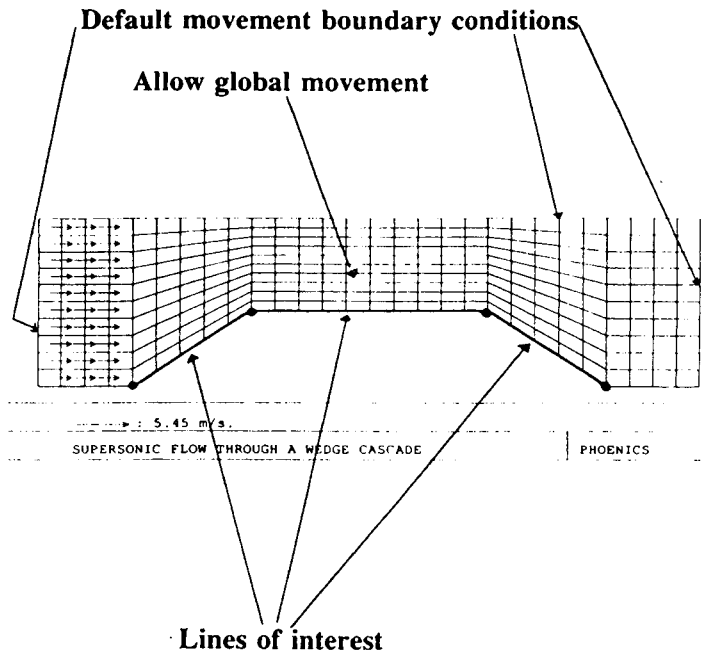

Figure 2. Regions of interest in a grid to be adapted

(vii) Proceed with the flow field solution until reasonable convergence is achieved.
(viii) Spline scalar field gradients and return to (i) until the grid stops changing.
(ix) In transient simulations, proceed to the next time step and repeat.

TEST COMPUTATIONS

A series of test examples exemplify the use of the adaptive technique developed. The list given in Table I includes subsonic, transonic and supersonic cases.

Table I. Test cases

Case	Description	Comments
1	Wedge cascade	Supersonic/inviscid
2	Converging–diverging Laval nozzle	Transonic
3	Missile nose-cone	Supersonic
4	Flow through a ball-valve	Subsonic
5	Cubic 'hill'	Potential flow
6	High-speed aerofoil	Transonic
7	Flow over a vertical plate	Subsonic

In all cases except the last, the field pressure was used as the controlling variable in the adaptive process. In case 7, the flow over a vertical plate, the velocity component in the main flow direction was chosen instead. In general the choice of variable will depend on the type of problem being solved.

The geometry outline of all test cases is given in Figure 3 and a brief description of each follows.

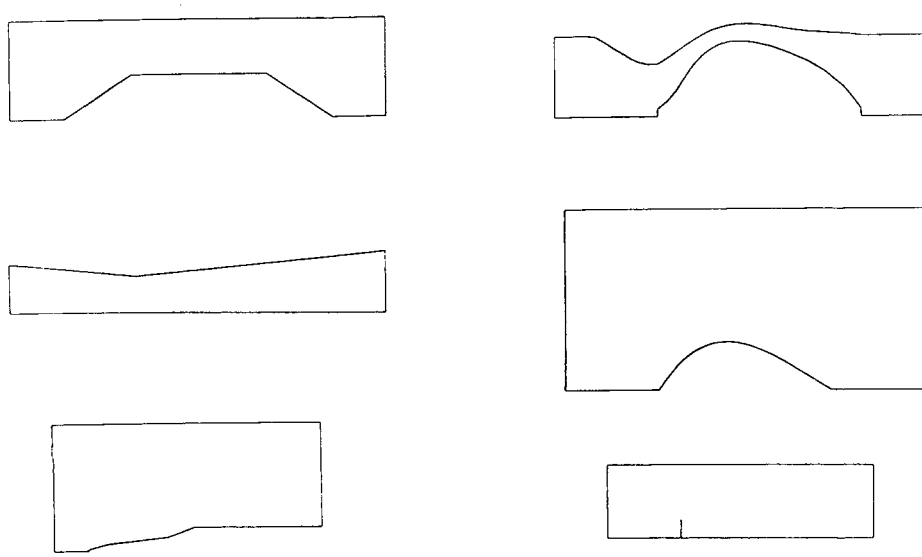

Figure 3. Geometry outline of test cases

1. Supersonic wedge cascade

This case is based on a PHOENICS library example. The flow considered is that through a cascade of wedges (see Figure 4) with an inlet Mach number of 3·0 and completely supersonic flow. An oblique leading edge shock reflects off the pressure surface of the wedge to be exactly cancelled at the upstream corner, giving a uniform parallel flow through the two surfaces. The flow then expands off the downstream corner and exits through the blade row, where two compression waves are formed at the trailing edge. Cyclic boundary conditions are applied upstream and downstream of the cascade.

The exit boundary condition is one of fixed pressure according to the post-expansion pressure calculated from gas dynamic theory; this neglects the presence of trailing edge shocks. This is only an approximate boundary condition, since the flow is hyperbolic, but sufficient for our purposes.

Figure 4(a) shows the initial coarse grid for this problem, produced by simple transfinite interpolation, and the inlet condition. Figure 4(b) shows the resulting pressure distribution after solution. The leading edge shock is shown quite clearly as a concentration of isobars. The reflected shock again is marked by isobars under the pressure surface of the adjacent aerofoil. Figures 4(c) and 4(d) show successive modifications of the grid caused by pressure gradients. The 'raw' move resulting from the application of the equidistribution method is shown without smoothing or correction for orthogonality. Grid lines are correctly attracted by the strong leading edge shock, but only mildly modified by other weaker features. Furthermore, the grid has become skewed in the region of interest. Figure 4 has been inserted to show that (a) the raw move alone can lead to unsuitable grids and (b) since the method adopted does not add more cells to the domain but simply redistributes the existing ones, an initially fine grid is desirable.

Figures 5 and 6 are for the same case but with a finer grid and Laplace-type orthogonalization. The grid development history is shown in a succession of plots. Grid adjustment takes place at a frequency of 10 flow field iterations. The grid and solution converge after about 300 iterative sweeps. A gradual cell enrichment process takes place in areas of rapid pressure variation, as a consequence of which the leading and reflected shock waves are well defined (Figure 6). In addition, the grid is much smoother and mostly orthogonal.

2. Transonic Laval nozzle

This case concerns plane, transonic flow through a convergent–divergent nozzle operating under design conditions. The nozzle geometry corresponds to a linear Mach number distribution as predicted by one-dimensional gas dynamic theory.

The inlet conditions are prescribed total pressure P_o and total temperature T_o at a Mach number of 0·5. The design outlet Mach number is 2·0, for which $P_{ex}/P_{o,1185in} = 0{\cdot}1278$. The exit boundary condition corresponds to a fixed pressure at the expected nodal Mach number. For values of P_{ex} greater than the design value the flow becomes subsonic through a normal shock compression. The shock position can be obtained analytically as a function of pressure ratio; in the case depicted, the shock occurs at 60 per cent chord.

Figure 7 shows the grid within the nozzle (only half modelled by symmetry) as it develops during adaption. As expected, the originally uniform grid converges towards the shock position; it is prevented from collapsing there by a user-defined minimum cell threshold. The grid is also modified in the throat region, where grid lines follow closely the shape of pressure contours (see Figure 9). Figure 8 shows the pressure distribution along the nozzle centreline as it varies with each grid adaption; the shock progressively sharpens with each move.

In order to see the effectiveness of the adaptive process in capturing the shock discontinuity, the pressure distribution is compared against that of the original grid and also against a calculation

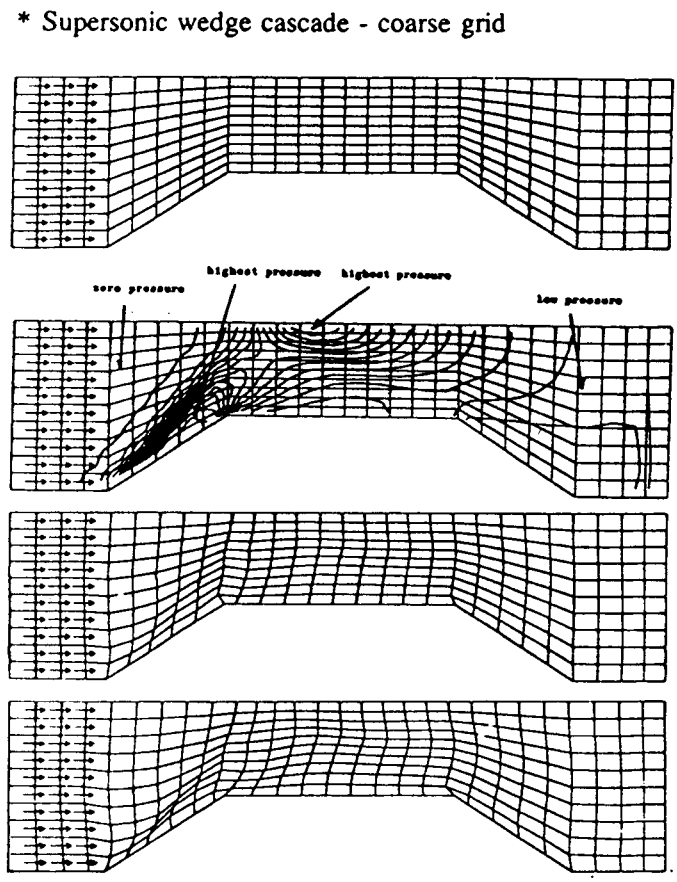

Figure 4. Wedge cascade: coarse grid—(a) initial grid; (b) resulting pressure; (c) moved grid no. 1; (d) moved grid no. 2

employing a shock-capturing scheme[16] in Plate 1. The closely packed isobars around the 60 per cent chord position mark the presence of a shock. This is considerably smeared in the original grid (Plate 1a) owing to simple upwind differencing. The introduction of a shock-capturing scheme (which, once a shock discontinuity is detected, prescribes the post-shock density to be that derived analytically, given the upstream conditions) sharpens the shock considerably (Plate 1b) but introduces solution convergence difficulties. Finally, the adaptive solution provides the sharpest discontinuity (Plate 1c) and requires fewer iterations than the other two methods. The difference can be seen more clearly in Figure 9, which depicts the pressure distribution along the nozzle centreline.

3. Missile nose-cone

The third case is axisymmetric and concerns the external flow past the front end of a supersonic missile featuring a complex cone nose section. The grid is initially uniform, with cross-streamlines being straight. The inlet velocity is prescribed at the upstream boundary, no-slip boundary conditions are assumed at the missile surface and the remaining boundaries are at a constant pressure.

Figure 10 shows the grid at two stages of adaption. Grid lines are bunched together in two distinct regions, one at the leading edge and the other just ahead of the cylindrical main body of the missile. Furthermore, the grid lines in these two regions incline with the flow to define two distinct cones. The

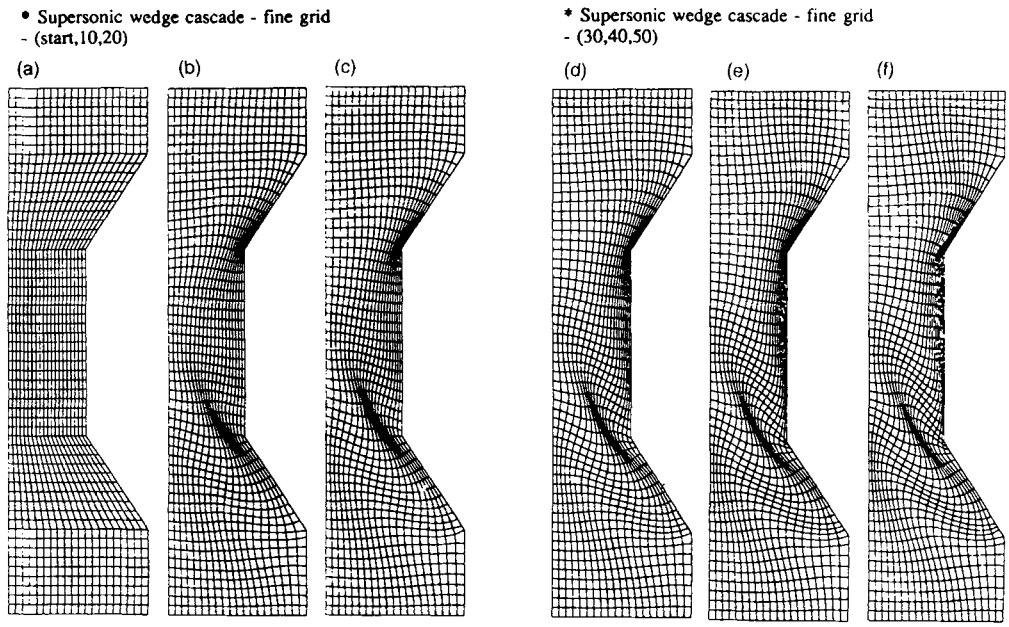

Figure 5. (a–f) Wedge cascade: fine grid history

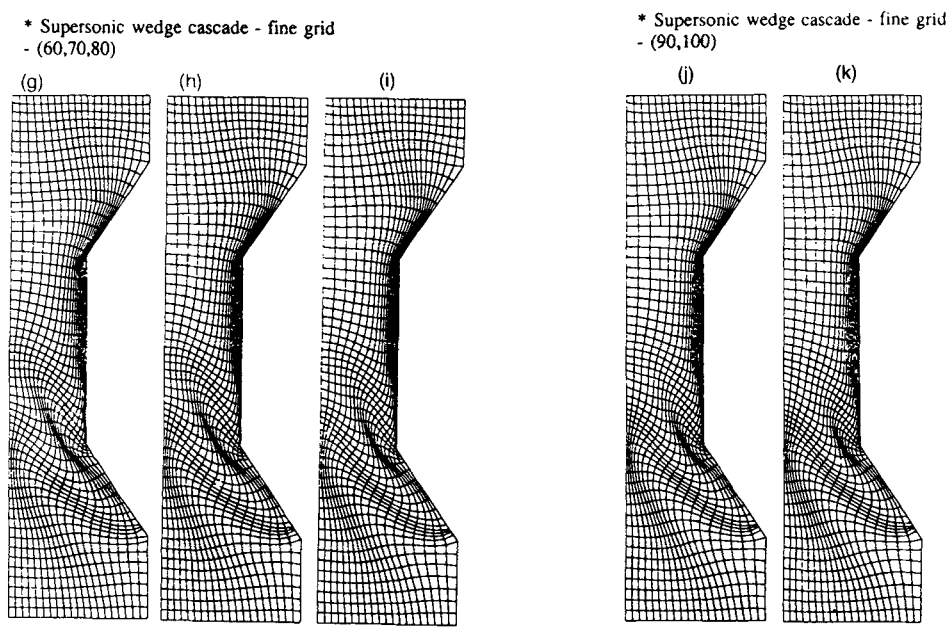

Figure 5. (g–k) Wedge cascade: fine grid history

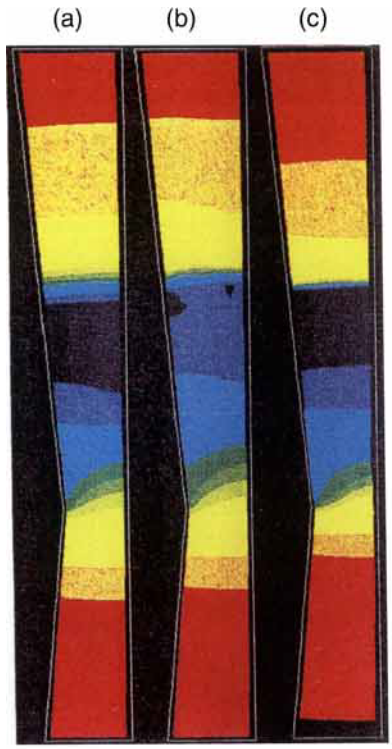

Plate 1. Laval nozzle: pressure fields for (a) standard, (b) shock capturing, and (c) adaptive methods

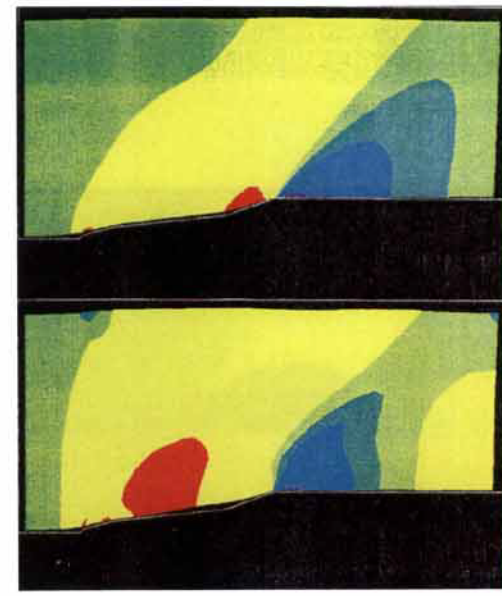

Plate 2. Missile nose-cone: contours of pressure

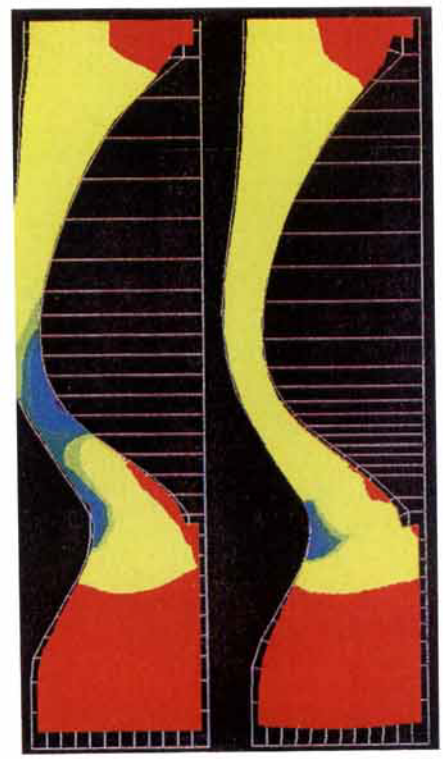

Plate 3. Ball valve: contours of pressure

Plate 4. Cubic hill: contours of pressure

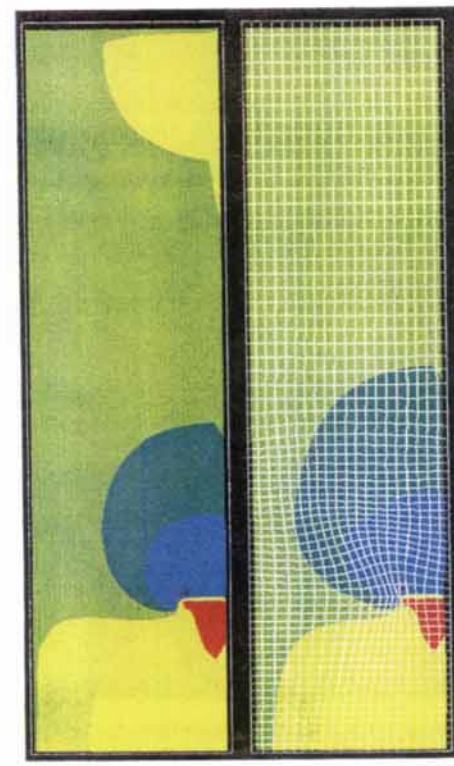

Plate 5. Vertical plate: grid before and after adaption including pressure fields

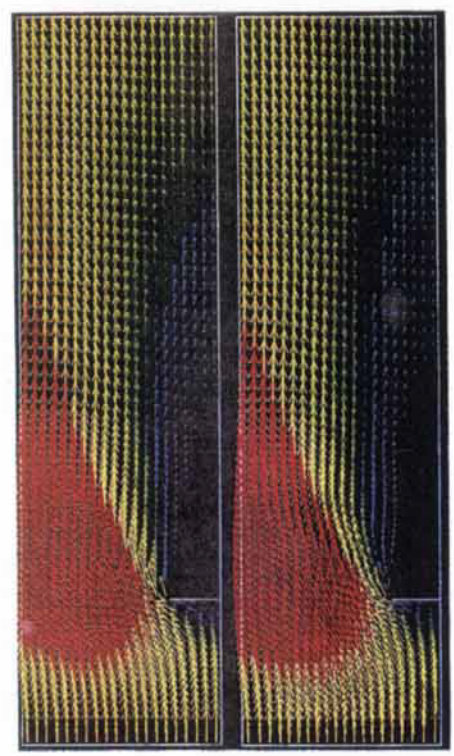

Plate 6. Vertical plate: velocity vectors and re-attachment streamline

Figure 6. Wedge cascade: fine grid pressure field

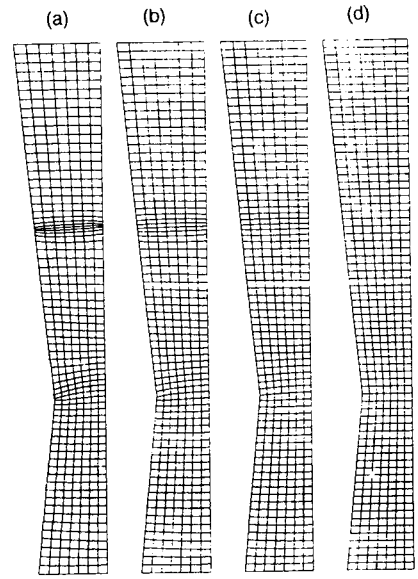

Figure 7. (a–d) Laval nozzle: grid development history

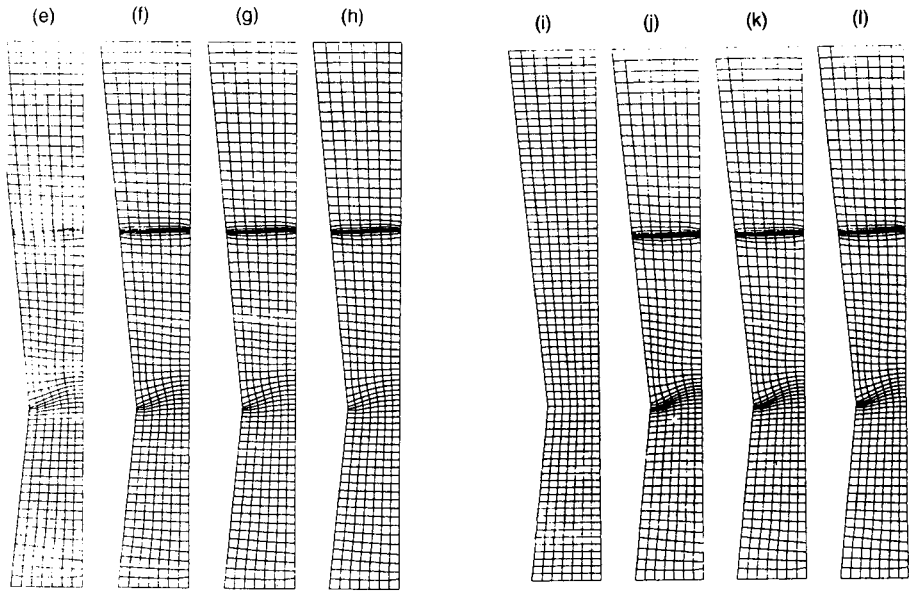

Figure 7. (e–l) Laval nozzle: grid development history

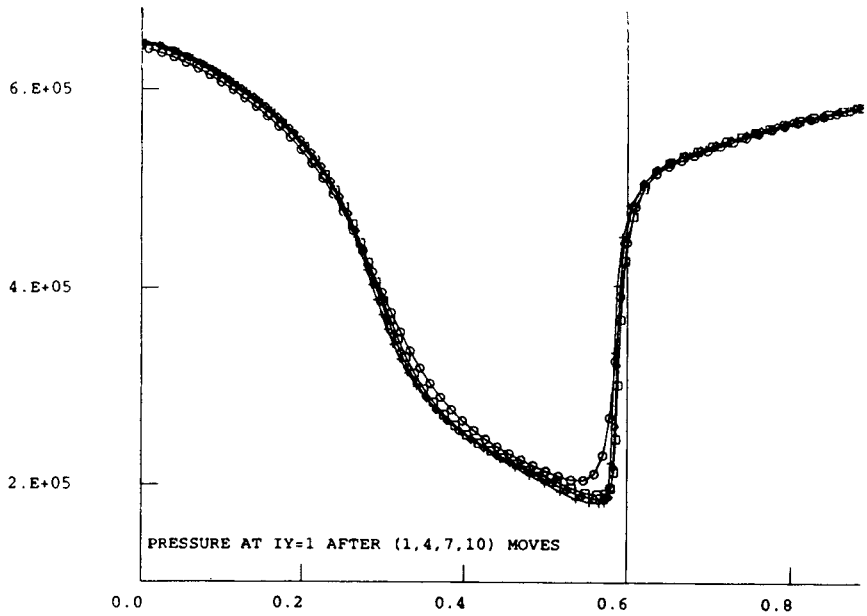

Figure 8. Laval nozzle: pressure development history

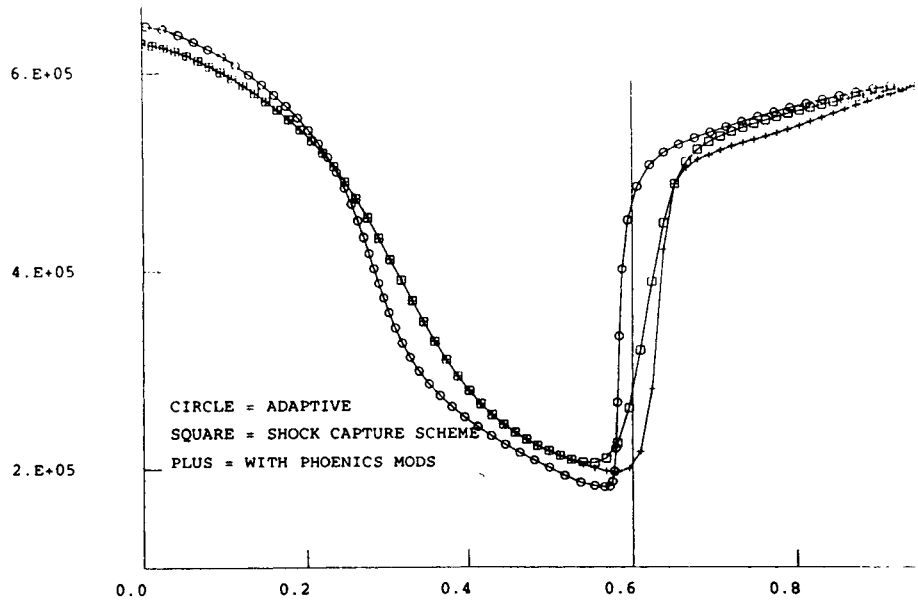

Figure 9. Laval nozzle: pressure distribution along central line— comparison of methods

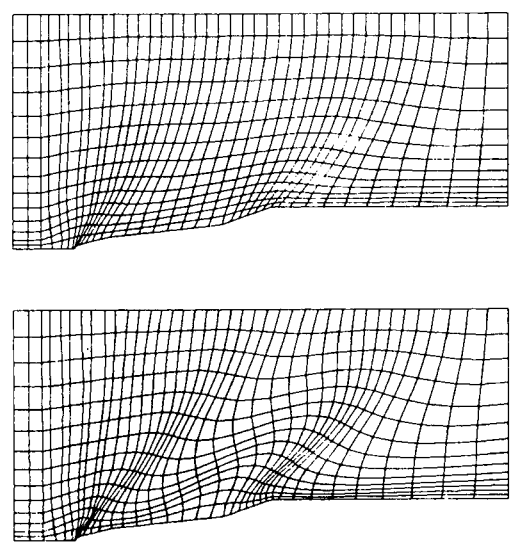

Figure 10. Missile nose-cone: grid development history—(a) initial; (b) moved

effect is clearly seen in Figure 10(b). Examination of the pressure field (Plate 2) shows the presence of two oblique shock waves separating alternating regions of low and high pressure.

4. Flow through a ball-valve

Again this is an axisymmetric problem, although the flow is now confined. The large blockage defining the inner boundary controls the flow through the valve by being moved axially. It is desirable to reduce head losses in such devices by preventing flow separation. Although this is a low-speed example, aeronautical equivalents can be found in the design of aero-engine nacelles.

The grid, shown in Figure 11, extends through the blocked region representing the ball. After a series of adaptions, grid lines are dragged towards the area of large pressure variation and seem to accumulate especially around the neck of the valve housing and on the shoulder of the ball. These positions coincide with areas where the flow accelerates and hence the pressure is low. The complex pressure field is shown in Plate 3.

5. Cubic 'hill' in a duct

The simple potential flow over a surface defined by a cubic polynomial is investigated next. Figure 12 shows the grid development history for this problem. The grid is originally uniform. As the computation proceeds, cells are attracted by the pressure gradient towards the maximum suction region, close to the position of maximum elevation. At the same time the Laplace-like solver attempts to draw grid lines away from the surface at the leading and trailing edges and towards it at mid-chord; the grid is obviously unsuitable as it stands for boundary layer studies. This case shows some of the weaknesses of the chosen approach. The authors are investigating alternative control functions which are more sensitive to surface curvature (see Figure 1). The pressure field for this simulation is shown in Plate 4.

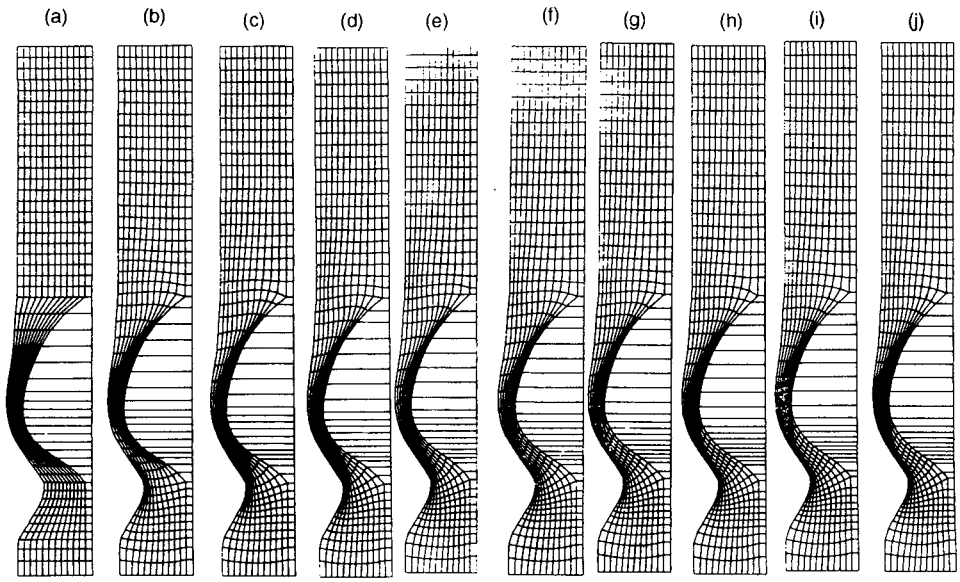

Figure 11. Ball-valve: grid development history

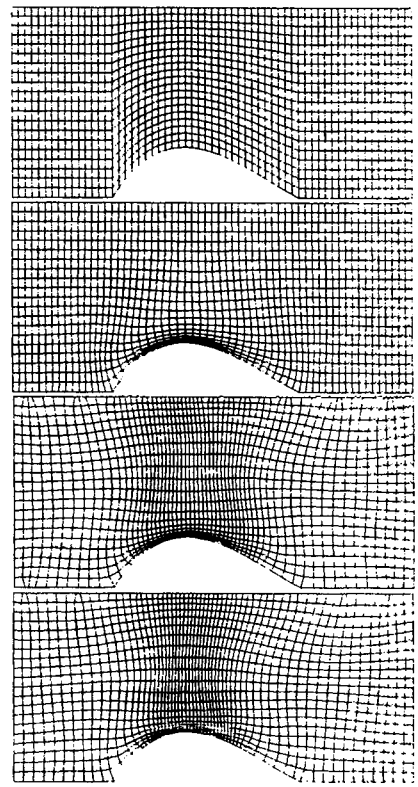

Figure 12. Cubic hill: grid development history

6. High-speed aerofoil in a duct

The hill of case 5 has been converted to a thin aerofoil by modifying the polynomial coefficients and simulated as a compressible flow problem. The initial and final grid distributions are shown in Figure 13. The grid is only mildly modified by the adaptive process. Nevertheless, the change is sufficient to increase the resolution of the oblique shock wave developing at the leading edge (see Figures 14(a) and (b)).

7. Flow over a vertical plate

In this case the interest lies in the separated flow region in the wake of a vertical plate. The flow is incompressible but viscous and turbulent. One of the problems one faces in simulating a problem such as this using CV techniques is numerical false diffusion—since the streamlines (or lines of mass flux) lie at an angle to the grid, influences propagate numerically in the cross-stream direction in a manner similar to viscous diffusion.[11,17] In the case of flow recirculation behind a step, false diffusion weakens the flow vorticity and reduces the reattachment length. High-order differencing schemes or even stream-directed differencing[18–20] have been used to alleviate this numerical defect. Often, however, the best solution is obtained by aligning the grid with the flow. This can be easily done using the adaptive grid facility.

Plate 5 shows the grid before and after adaption. The axial velocity gradient is now the driving force behind grid movement. The grid is seen to 'bend' in the direction along the main flow direction at the

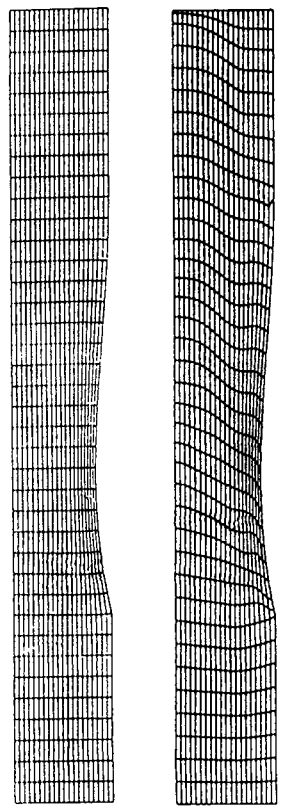

Figure 13. High-speed aerofoil: grid

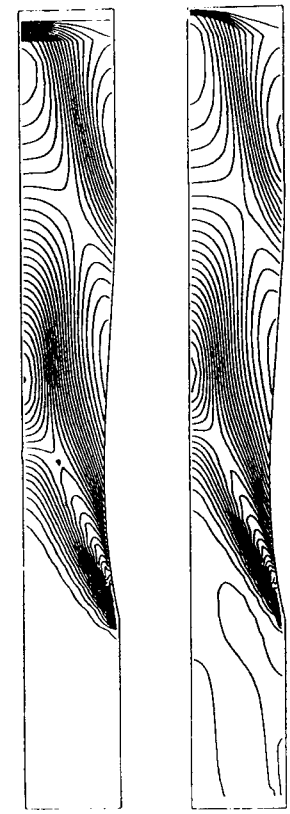

Figure 14. High-speed aerofoil: contours of pressure

plate edge. This small alteration results in a significant change in the computed flow field; in particular, the position of reattachment moves further downstream, from x- to y-plate heights (see Plate 6), as less of the deflected flow momentum is dissipated by false diffusion.

In all the cases described above, a field variable has been used to effect the adaption. This is not always necessary, as demonstrated in Figures 15 and 16, where a geometric quantity (i.e. height above a datum) has been used instead to modify a three-dimensional surface grid describing the intersection of two cylinders. The initially uniform grid has been attracted towards regions of high height gradient by applying one of the Wx-functions of Figure 1. For further details of its full formulation and its application in two and three dimensions, see Reference 21.

CONCLUDING REMARKS

This paper has described work performed at the University of Greenwich (formerly Thames Polytechnic) to develop a generic adaptive grid facility for a CV-type structured grid CFD code. The motive behind this work was primarily to improve the shock-capturing capability of such codes, which are widely used for viscous compressible aerodynamic simulations without resort to expensive and often uncertain explicit time-marching techniques.

The fully automatic adaptive facility which has been created has various elements which allow the creation of a numerically suitable grid which is at the same time sensitive to flow variables and economical in use. These are as follows.

1. The total number of cells in a single calculation remains constant; local grid refinement is by redistribution. This is in contrast with the practice commonly adopted by finite element workers, who tend to enrich the grid locally by node addition.
2. Grid movement is by gradient equidistribution and subsequent normalization.
3. Surface-tracking facilities have been introduced using bi-cubic splines or alternatively user-defined functions to ensure surface definition is not compromised by grid movement.
4. The patch-wise use of a Laplace grid solver ensures that grids maintain orthogonality for numerical accuracy. However, care has to be exercised where fine grids are required close to a surface (e.g. for boundary layer calculations), since the Laplace solver tends to pull cells away from concave surfaces.
5. The adaptive process is iterative and automatic. User input is restricted to the initial grid creation

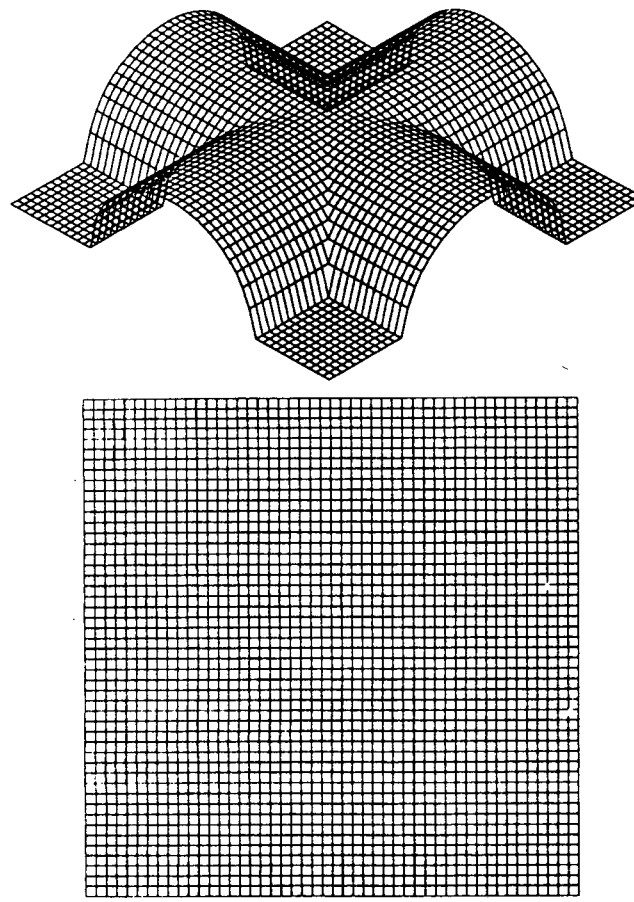

Figure 15. Cylinder junction: initial grid

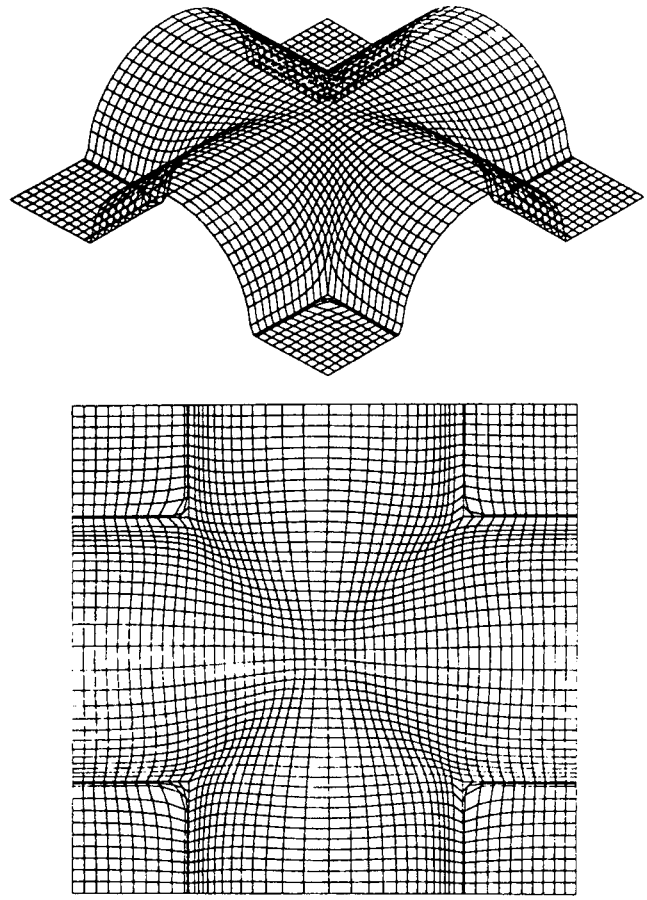

Figure 16. Cylinder junction: adapted grid

and to the specification of the problem geometry as a series of discrete surface patches and fixed points.

6. The user can adapt the grid on any variable, enabling the application of the technique to many problems in a general-purpose CFD code.

The technique has been applied to a series of test examples with interesting results. Using pressure or other variables as the driving field variable, shock resolution has been enhanced. Solution convergence has in most cases improved with grid adaptivity, since the fineness of discretization now reflects flow activity; this removes disproportionally large residual errors often encountered in badly distributed grids. In general the adaptive procedure requires the equivalent of two sweeps of the computational fluid dynamics code per adaption, but this can vary greatly depending on the initial grid distribution, the adaption variable and the choice of the adaptive control parameters. This translates to a modest increase in CPU time over the static solution. An unexpected outcome of this study has been the realization that adaptive grids can reduce false diffusion in multidimensional simulations simply by aligning grid lines with the local flow direction—the authors are further investigating this capability.

Many applications not mentioned here can benefit from an adaptive grid option. Examples include

free surface problems, flame fronts and detonation waves in gaseous combustion, jets and shear layers, phase change interface tracking and many more.

Finally it should be mentioned that the accuracy of the final solution depends to a large extent on how grid-independent the results are; although this may be stating the obvious, care must be exercised to ensure that the starting grid is fine enough for the job at hand before attempting to adapt it.

APPENDIX: NOMENCLATURE

Δx	new cell dimension
Δx_o	original cell dimension
Δx_n	new cell dimension
Δx_{min}	minimum allowable cell dimension
Δx_{max}	maximum allowable cell dimension
k	constant
k_x	x-direction
ϕ	dependent variable
α	cell contraction parameter
nx	number of cells in x-direction
ny	number of cells in y-direction
nz	number of cells in z-direction

REFERENCES

1. A. Jameson, 'Transonic aerofoil calculations using the Euler equations', in P. L. Roe (ed.), *Numerical Methods in Aeronautical Fluid Dynamics*, Academic, London, 1982, pp. 289–309.
2. A. Jameson, 'A vertex based multigrid algorithm for three dimensional compressible flow calculations', *ASEM WAM*, Anaheim, CA, 1986, pp. 45–73.
3. S. V. Patankar and D. B. Spalding, 'A calculation procedure for heat, mass and momentum transfer in three-dimensional parabolic flows', *Int. J. Heat and Mass Transfer*, **15**, 1787 (1972).
4. J. P. Van Doormal, G. D. Raithby and B. H. McDonald, 'The segregated approach to predicting viscous compressible fluid flows', *ASME J. Turbo Machinery*, **109**, 268–277 (1987).
5. C. M. Rhie and S. T. Stowers, 'Navier–Stokes analysis for high speed flows, using the pressure correction algorithm', *AIAA Paper 87-1980*, 1987.
6. S. Wornom and M. Hafez, 'Calculations of quasi-one dimensional flows with shocks', *Comput. Fluids*, **14**, 131–140 (1986).
7. J. J. McGurik and G. J. Page, 'Shock capture using a pressure correction method', *AIAA J.*, **28** (1990).
8. H. I. Rosten and D. B. Spalding, 'The PHOENICS reference manual', *CHAM TR/200*, CHAM Ltd., London, 1987.
9. A. Evans, M. J. Marchent, J. Szmelter and N. P. Weatherill, 'Adaptivity for compressible flow computations using point embedding on 2-D structured multiblock meshes', *Int. j. numer. methods eng.*, **32**, 895–910 (1991).
10. J. S. Mathur and N. P. Weatherill, 'The simulation of inviscid, compressible flows using an upwind kinetic method on unstructured grids', *Int. J. Numer. Methods Fluids*, **15**, 59–82 (1992).
11. S. V. Patankar, *Numerical Heat Transfer and Fluid Flow*, McGraw-Hill, Washington, DC, 1980.
12. K. Nakahashi and G. S. Geiwert, 'A self-adaptive grid method with applications to aerofoil flows', *AIAA Paper 85-1525*, 1985.
13. D. Catherall, 'The adaptation of structured grids to numerical solutions for transonic flow', *Int. j. numer. methods eng.*, **32**, 921–937 (1991).
14. K. A. Pericleous, E. N. Jal and D. R. Glynn, 'Numerical prediction of flow entrainment around V/STOL aircraft in hover', *Proc. Int. Aerospace Conf. and Exhib.*, Athens, October 1990.
15. L. S. Caretto, A. D. Gosman, S. V. Patankar and D. B. Spalding, 'Two calculation procedures for steady, three-dimensional flows with recirculation', in J. Ehlers, K. Hepp and W. A. Wedemuller (eds), *Proc. Third Int. Conf. on Numerical Methods in Fluid Dynamics*, Vol. 11, Springer, Heidelberg, 1972, p. 60.
16. K. A. Pericleous and M. K. Patel, 'A simple physical shock capturing technique', *University of Greenwich Internal Rep. CNMP/BAe/4-1*, 1992.
17. G. De Vahl Davis and G. D. Mallinson, 'An evaluation of upwind and central difference approximations by a study of recirculating flow', *Comput. Fluids*, **4**, 24–43 (1976).
18. M. K. Patel, M. Cross and N. C. Markatos, 'A critical evaluation of seven-discretization schemes for convection–diffusion equations', *Int. j. numer. methods fluids*, **5**, 225–244 (1985).
19. M. K. Patel, M. Cross, N. C. Markatos and C. Mace, 'An evaluation of eleven-discretization schemes for predicting elliptic flow and heat and mass transfer in supersonic jets', *Int. J. Heat Mass Transfer*, **30**, 1907 (1987).
20. M. K. Patel, M. Cross and N. C. Markatos, 'An assessment of flow-oriented schemes for reducing false-diffusion', *Int. j. numer. methods fluids*, **26**, 2279–2304 (1988).
21. C. R. Bennett, 'Grid adaption using the Laplace–Poisson–equidistribution (LPE) equation', M.Sc. Thesis, University of Greenwich, 1992.